

Tallal HAKMI <sup>1</sup>, Amine HAMDI <sup>1</sup>, Youssef TOUGGUI <sup>2,3</sup>,  
Aissa LAOUISSI <sup>4</sup>, Salim BELHADI <sup>3</sup>, Mohamed A. YALLESE <sup>3</sup>

## Machinability investigation during turning of polyoxymethylene POM-C and optimization of cutting parameters using Pareto analysis, linear regression and genetic algorithm

Received 29 July 2023, Revised 26 December 2023, Accepted 3 January 2024, Published online 8 March 2024

**Keywords:** turning, POM-C, Pareto chart, multiple regression, genetic algorithm

This paper presents a study on the dry turning of polyoxymethylene copolymer POM-C. The effect of five factors (cutting speed, feed rate, depth of cut, nose radius, and main cutting edge angle) on machinability is evaluated using four output parameters: surface roughness, tangential force, cutting power, and material removal rate. To do so, the study relies on three approaches: (i) Pareto statistical analysis, (ii) multiple linear regression modeling, and (iii) optimization using the genetic algorithm. To conduct the investigation, mathematical models are developed using response surface methodology based on the Taguchi  $L_{16}$  orthogonal array. The results indicate that feed rate, nose radius, and cutting edge angle significantly influence surface quality, while depth of cut, feed, and speed have a notable impact on other machinability parameters. The developed mathematical models have determination coefficients greater than or very close to 95%, making them very useful for the industry as they allow predicting response values based on the chosen cutting parameters. Finally, the optimization using the genetic algorithm proves to be promising and effective in determining the optimal cutting parameters to maximize productivity while improving surface quality.

---

✉ Tallal HAKMI, e-mail: [talal.hakmi@univ-tissemst.dz](mailto:talal.hakmi@univ-tissemst.dz)

<sup>1</sup>Laboratory of Mechanical Engineering, Materials and Structures, Tissemst University, Algeria

<sup>2</sup>Applied Mechanics and Energy Systems Laboratory, Faculty of Applied Sciences, Kasdi Merbah Ouargla University, Algeria

<sup>3</sup>Mechanics and Structures Research Laboratory (LMS), Guelma, Algeria

<sup>4</sup>Mechanics Research Centre, Constantine, Algeria



© 2024, The Author(s). This is an open-access article distributed under the terms of the Creative Commons Attribution (CC-BY 4.0, <https://creativecommons.org/licenses/by/4.0/>), which permits use, distribution, and reproduction in any medium, provided that the author and source are cited.

## 1. Introduction

Nowadays, one of the main challenges for researchers and industries is to find alternatives to metals by using other materials. In this context, industry 4.0 technology aims to significantly increase the demand for polymer materials, particularly in mechanical manufacturing [1]. This surge is attributed to their unique and specific properties when compared to metals. Commonly observed properties in polymers include improved stiffness and strength, as seen in polyacetal (POM-C), high resistance to corrosion and oxidation, excellent electrical and thermal insulation, high resistance to degradation from heat, UV radiation, chemicals, and other environmental factors, low density, and ease of processing. Additionally, polymers can be molded, extruded, laminated, cut, and formed into a variety of shapes and sizes, ... etc. [1, 2]. Due to these properties, polymers are increasingly being used in various engineering fields such as automotive [3], robotics [4], aerospace [5], and machinery [6]. Mechanical parts used in these fields include gears, wheels, bearings, and rolling elements [1, 7, 8].

At present, large-scale polymer manufacturing processes vary depending on the type of polymer and its intended application. However, common methods used to produce these technical materials include chain polymerization, addition polymerization, condensation polymerization, and ring-opening polymerization. Extrusion molding is used to produce polymers such as high-density polyethylene (HDPE) [9]. Injection molding is also a common method to produce precision plastic parts. There are also other methods, such as blow molding, compression molding, transfer molding, and rotational molding, which are used to produce plastic parts with different shapes and properties [10]. Producing small quantities of high-quality micro-components with complex geometries and good surface integrity poses a manufacturing challenge for mechanical parts [11]. However, the demand for such products is on the rise due to a design focus on reducing on-board masses. Conventional processes are often limited and cannot meet the specific requirements of the design. Furthermore, these processes are often associated with high costs and longer lead times [10, 12]. Therefore, the use of material removal machining processes such as turning, milling, and drilling of plastics is increasing. These processes enable the efficient, high-precision, rapid, and cost-effective production of complex mechanical parts [11, 12].

For many years, there has been a continuing interest in the surface finish quality of polymer parts, as improving surface texture by reducing roughness is essential for achieving optimal performance in machined components. Various factors influence the surface finish of machined part, but cutting speed ( $V_c$ ), feed rate ( $f$ ), and depth of cut ( $ap$ ) are the primary machining factors that have a significant influence on surface roughness under given conditions [13]. Within this context, Hamlaoui et al. [14] studied the machinability of high-density polyethylene (HDPE) used in the production of pipes and mechanical test specimens. Classical turning parameters ( $V_c$ ,  $f$ , and  $ap$ ) were used as factors, with three surface roughness criteria ( $R_a$ ,

$R_t$ , and  $R_z$ ) and cutting temperature as responses. The results showed that the feed rate ( $f$ ) is the main factor contributing to minimize the surface roughness of HDPE material. On the other hand, the cutting temperature is mainly influenced by cutting speed ( $V_c$ ), depth of cut ( $ap$ ), and their interactions. According to two studies conducted by Cabrera et al. [15, 16], feed rate ( $f$ ) and depth of cut ( $ap$ ) are the two independent variables with the greatest influence on surface roughness during CNC turning of polyetheretherketone (PEEK CF30) polymer using a TiN-coated tool. These authors emphasize the importance of selecting appropriate machining parameters to achieve a high-quality surface finish using two optimization methods: the Taguchi method and the gray relational analysis (Taguchi-GRA). Additionally, fuzzy logic-based modeling appears as a highly effective method for predicting the two dependent variables ( $Ra$  and  $Rt$ ). Similar results were obtained by Akkuş and Yaka [17] when turning titanium alloy (Ti 6Al-4 V, grade 5). They showed that the feed rate was the key parameter to obtain a surface with minimal  $Ra$  parameter, while the cutting speed was the key parameter to control tool wear.

Determining cutting forces in material removal machining is a major challenge in manufacturing industry as well as in scientific research. To investigate the generation of cutting forces and model them using artificial neural network (ANN), Özden et al. [18] conducted a study on turning unreinforced and reinforced polyamide (PA) with 30% carbon fiber. Two cutting tools (K15 (DCMW 11T304H13A) and PCD (DCMW 11T3 04FPDC10)) were employed, along with a full factorial design (FFD). The results from training and testing the artificial neural network (ANN) model show a good correlation between predicted values and experimental data. In this regard, the study by Gaitonde et al. [19] explored the effect of cutting parameters on 30% glass fiber reinforced polyamide (PA66-GF30) and unreinforced polyamide (PA6). The ANN models showed that it is essential to set high values of the feed rate ( $f$ ) and cutting speed ( $V_c$ ) when machining PA66-GF30 in order to reduce the specific cutting force ( $K_c$ ). In another investigation, Baroiu et al. [20] evaluated the surface roughness of three polymers commonly used in industry and scientific research: high-density polyethylene (HDPE 1000), nylon 6 (PA 6), and polyoxymethylene (POM-C). They used two high-speed steel HS18-0-1 helical drills of different diameters ( $\varnothing 8$  and  $\varnothing 10$  mm) for the drilling operations, while keeping the same cutting conditions for all three materials. The results showed that POM-C produced the best surface quality, followed by HDPE 1000 and PA6, respectively. Interestingly, Tabacaru et al. [21] conducted the previous machining process for the same materials in order to model the surface roughness ( $Ra$ ) using the ANN method. The authors arrived at the same conclusion as the previous study [20], namely that POM-C has the best machinability, followed by HDPE 1000 and PA6.

The literature indicates that polymer machining is less studied than metal machining, including for polyoxymethylene copolymer POM-C, an industrial plastic widely used, yet not sufficiently investigated in recent machining research. The existing studies on polymer turning generally focus on conventional cutting param-

eters such as cutting speed  $V_c$ , feed rate  $f$ , and depth of cut  $ap$ , but do not address cutting tool parameters such as nose radius ( $r_\epsilon$ ) and principal cutting edge angle ( $X_r$ ). In this context, the objective of this study is to present a machinability study of POM-C using five input parameters:  $V_c$ ,  $f$ ,  $ap$ ,  $r_\epsilon$ , and  $X_r$ . This study evaluates the impact of these factors on surface quality ( $Ra$ ), tangential force ( $F_Z$ ), cutting power ( $P_c$ ), and material removal rate ( $MRR$ ) using three approaches: a Pareto statistical analysis to identify the most significant factors on each machinability parameter, a multiple linear regression modeling, and an optimization by the genetic algorithm (GA) to obtain the optimal cutting parameters. The models are evaluated using the coefficient of determination ( $R^2$ ) and the mean absolute percentage error (MAPE).

## 2. Experimental procedure

### 2.1. Workpiece material

The material used for the turning tests is polyoxymethylene (POM-C), a polymer commonly used in the mechanical industry. Specimens measuring 300 mm in length and 80 mm in diameter were provided by the German company Ensinger. POM-C, also known as acetal, is a copolymer produced through the copolymerization of acetone and formaldehyde  $(CH_2O)_n$ . The noteworthy properties of this plastic are outlined in Table 1.

Table 1. Technical properties of POM-C

1. Mechanical properties	Value
Tensile strength (MPa)	67
Elongation at break (%)	32
Notch impact strength (KJ/m <sup>2</sup> )	8
Hardness (ball) (MPa)	165
Flexural strength (MPa)	91
Modulus of elasticity (MPa)	2800
2. Thermal properties	Value
Thermal conductivity (W/(k·m))	0.39
Specific heat (J/(g·K))	1.4
Thermal expansion coefficient ( $\alpha$ ) (K <sup>-1</sup> · 10 <sup>-5</sup> )	13
Glass transition temperature ( $T_g$ ) (°C)	-60
Melting temperature $T_M$ (°C)	166
Service temperature (°C)	140

The POM-C exhibits high mechanical strength in tension, compression, and bending, consistent dimensional stability under varying mechanical loads and temperature changes, heat resistance, good chemical resistance, low moisture absorption, and excellent dimensional stability. Polyacetal is a high-performance thermoplastic that is commonly used in various industrial applications such as mechanical parts, bearings, gears, sleeves, pump housings, wheels, and slides.

## 2.2. Machine-tool and cutting tool

Turning operations were performed on a conventional TOS TRENCIN machine tool (model SN 40C) with a spindle power of 6.6 kW. The rotational speeds range of this machine varies from 45 to 2000 rpm, while feed rates can range from 0.08 to 6.4 mm/rev.

For the turning operations of POM-C polymer samples, two single-sided positive turning inserts were used: SPMR 120304 ( $r_\epsilon = 0.4$  mm) and SPMR 120308 ( $r_\epsilon = 0.8$  mm) from the company Dormer Pramet. These inserts belong to grade T9325 and are made from a functionally MT-CVD coated functionally graded WC-Co carbide within ISO ranges P15-P35, with four cutting edges for each insert. The main geometric feature is a clearance angle  $\alpha_{0i}$  of  $11^\circ$ . In addition, the tool holders used to hold and position the inserts are CSDPN 2525M12 (with a cutting edge angle  $X_r$  of  $45^\circ$ , a rake angle  $\gamma_{0h}$  of  $6^\circ$ , and an inclination angle  $\lambda_s$  of  $0^\circ$ ), CSBPR 2525M12 (with a cutting edge angle  $X_r$  of  $75^\circ$ , a rake angle  $\gamma_{0h}$  of  $6^\circ$ , and an inclination angle  $\lambda_s$  of  $0^\circ$ ).

Careful selection of geometry can improve productivity, surface quality and tool life. Therefore, the characteristics of the inserts, tool holders and the levels of variation in cutting conditions are selected in accordance with the recommendations of the plastic manufacturer Ensinger and the tool manufacturer Dormer Pramet.

## 2.3. Design of experiments and cutting parameters

The study of material removal machining processes has become increasingly complex due to the large number of input parameters that can influence one or more responses. The experimental complexity lies in establishing the experimental design, which determines the number of samples to be tested based on the influences and interactions being studied. Additionally, it will be necessary to create the samples and conduct the tests.

To address this challenge, it is necessary to adopt a rigorous approach in conducting the tests, applying the design of experiments (DOE) method that provides an efficient approach to solve complex problems. Table 2 shows the selected independent variables and the associated ranges of variation for each of them. According to this table, we have four levels for the three classic input parameters ( $V_c$ ,  $f$ , and  $a_p$  ( $4^3$ )), and two levels for the cutting tool geometry factors ( $r_\epsilon$  and  $X_r$  ( $2^2$ )). Therefore, the total number of experiments to examine all the interactions

between the five factors amounts to 256. Thus, the Taguchi experimental design method ( $L_{16} = 4^3 \times 2^2$ ) has been selected to establish an experimental plan that requires the minimum number of tests possible based on the desired information. This allows for a reduction in costs associated with testing, while ensuring that POM-C samples are subjected to machining conditions that are representative of the real-world industrial settings.

Table 2. Cutting conditions and their variation ranges

Parameters	Level 1	Level 2	Level 3	Level 4
$V_c$ [m/min]	240	300	360	420
$f$ [mm/rev]	0.08	0.14	0.20	0.24
$ap$ [mm]	0.8	1.6	2.4	3.2
$r_\varepsilon$ [mm]	0.4	0.8	–	–
$X_r$ [°]	45	75	–	–

#### 2.4. Measurement configuration

The average arithmetic roughness measurement ( $Ra$ ) was taken using a Mitutoyo Surftest-201 roughness tester equipped with a probe that had a 5  $\mu\text{m}$  radius diamond tip. The evaluation length  $L_n = 2.4$  mm and the cut-off wavelength  $\lambda_c = 0.8$  mm were used. Each test was characterized by three measurements taken at different locations separated by an angle of 120°, and the average value was taken to provide greater reliability to the results. The cutting forces was measured using a Kistler piezoelectric dynamometer (model 9257B) connected through a multi-channel load amplifier (type 5011B). Fig. 1 represents the details of the experimental step.

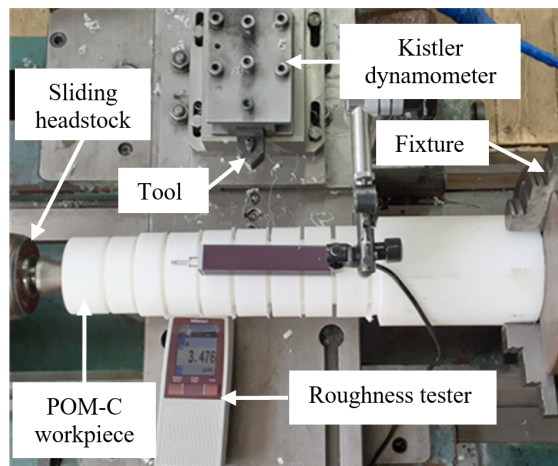


Fig. 1. Details of the experimental step

### 3. Results and discussion

The experimental results encompass various measurements, including arithmetic mean roughness ( $Ra$ ), tangential force ( $F_Z$ ), cutting power ( $P_c$ ), and material removal rate ( $MRR$ ). These results are based on five factors considered in this study ( $V_c$ ,  $f$ ,  $ap$ ,  $r_\varepsilon$ , and  $X_r$ ), and are represented in Table 3. Cutting power ( $P_c$ ) and material removal rate ( $MRR$ ), the third and last machinability parameters, are calculated using Eqs. (1) and (2) respectively.

$$MRR = V_c \cdot f \cdot ap \quad (\text{cm}^3/\text{min}), \quad (1)$$

$$P_c = \frac{F_z V_c}{60} \quad (\text{W}). \quad (2)$$

Table 3. Experimental results of  $Ra$ ,  $F_Z$ ,  $MRR$ , and  $P_c$  as a function of cutting parameters

No	Input factors					Responses			
	$V_c$ [m/min]	$f$ [mm/rev]	$ap$ [mm]	$r_\varepsilon$ [mm]	$X_r$ [°]	$Ra$ [μm]	$F_Z$ [N]	$MRR$ [cm <sup>3</sup> /min]	$P_c$ [W]
1	240	0.08	0.8	0.4	45	2.47	13.56	15.36	54.24
2	240	0.14	1.6	0.4	45	3.10	45.65	53.76	182.60
3	240	0.20	2.4	0.8	75	2.15	80.71	115.20	322.84
4	240	0.24	3.2	0.8	75	2.92	113.04	184.32	452.16
5	300	0.08	1.6	0.8	75	1.01	24.20	38.40	121.00
6	300	0.14	0.8	0.8	75	1.30	25.30	33.60	126.50
7	300	0.20	3.2	0.4	45	4.00	105.56	192.00	527.80
8	300	0.24	2.4	0.4	45	5.05	88.67	172.80	443.35
9	360	0.08	2.4	0.4	75	1.35	38.22	69.12	229.32
10	360	0.14	3.2	0.4	75	2.35	75.30	161.28	451.80
11	360	0.20	0.8	0.8	45	2.52	24.90	57.60	149.40
12	360	0.24	1.6	0.8	45	2.99	65.30	138.24	391.80
13	420	0.08	3.2	0.8	45	0.60	59.71	107.52	417.97
14	420	0.14	2.4	0.8	45	1.32	60.12	141.12	420.84
15	420	0.20	1.6	0.4	75	3.27	49.14	134.40	343.98
16	420	0.24	0.8	0.4	75	3.98	35.25	80.64	246.75

#### 3.1. Statistical Pareto analysis

A Pareto chart is a graphical tool used to visually represent the distribution of causes within a dataset based on their relative importance. It is based on the principle of Pareto's law, also known as the 80/20 rule, which states that 80% of effects are caused by 20% of the causes. The chart consists of a vertical axis

representing the impact of each cause and a horizontal axis ranking the causes in descending order of importance. The most significant causes are shown on the left side, while less critical ones are on the right. Widely used in quality management, decision-making, and problem-solving, the Pareto chart assists in identifying the most crucial causes that should be addressed first, improving overall system efficiency. Pareto analysis, as a statistical tool, is valuable for determining the significant effect of each input parameter on output responses [22, 23].

### 3.1.1. Surface roughness ( $Ra$ )

Surface roughness is a key parameter in machining, exerting a significant impact on the quality and performance of machined parts. Its influence extends to factors such as friction, adhesion, wear, fatigue resistance, corrosion, lubrication, and overall functionality of the machined part. In Fig. 2, a Pareto analysis of the arithmetic mean roughness ( $Ra$ ) is applied to find the main factors in order to ensure better precision on machined POM-C parts. According to this plot, the most important factors are located on the left-hand side of the graph, namely the feed rate ( $f$ ) and the nose radius ( $r_\epsilon$ ), with contributions of 58.05% and 32.25%, respectively. The principal direction angle ( $X_r$ ) is located in the middle of the graph with a small contribution of 3.86%. On the other hand, the cutting speed ( $V_c$ ) and the depth of cut ( $ap$ ) are located on the right-hand side, indicating that these two independent variables are the least important. In fact, the value of  $F$  for  $ap$  (0.49%) is below the limited confidence level line (2.23%), indicating that this factor has no significant impact on the  $Ra$  response. According to Chabbi et al. [7, 8], the second factor that affects surface roughness during turning of the same polymer is the depth of cut, with a contribution of 19.70% after the feed rate, which is the main factor with a contribution of 66.41% obtained by the analysis of variance

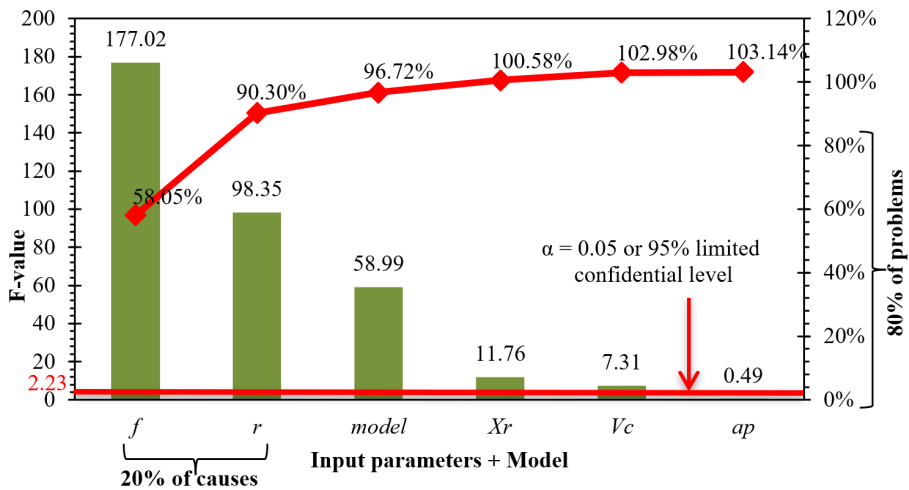


Fig. 2. Pareto chart of  $Ra$

(ANOVA). The cutting speed is also significant, but its contribution is low (5.28%). In a previous study, it was observed that when turning PA66 polyamide, the feed rate was the most important factor affecting the  $Ra$  parameter [24].

### 3.1.2. Tangential force ( $F_Z$ )

Cutting forces are of paramount importance in the process of removing material from polymer workpieces, and machining these materials can be challenging due to unique properties such as their elasticity and sensitivity to heat. Fig. 3 shows the Pareto chart for the cutting force  $F_Z$  to investigate systematically the effect of five independent variables on this second machinability parameter. To improve the cutting force, the two most important input parameters to address first are the depth of cut ( $ap$ ) and the feed rate ( $f$ ), contributing 66.48% and 28.69%, respectively, according to this analysis. Cutting speed ( $V_C$ ) has a lower contribution at 4%, while the two cutting tool factors ( $X_r$  and  $r_\epsilon$ ) on the right side of the graph show not significant on the dependent variable  $F_Z$ . These results are consistent with the conclusions of Chabbi et al. [7, 8]. According to Gaitonde et al. [19], the cutting force ( $F_Z$ ) strongly depends on the feed rate ( $f$ ), rather than the cutting speed ( $V_C$ ), during the turning of polyamide PA 6.

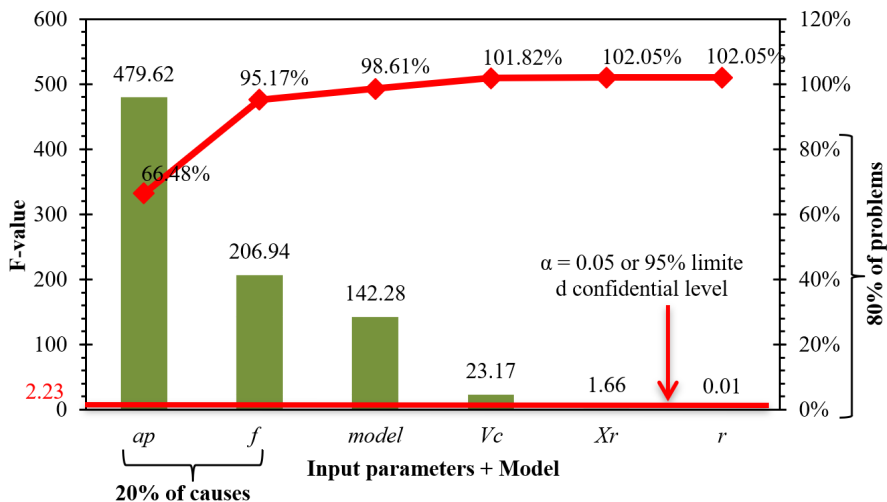
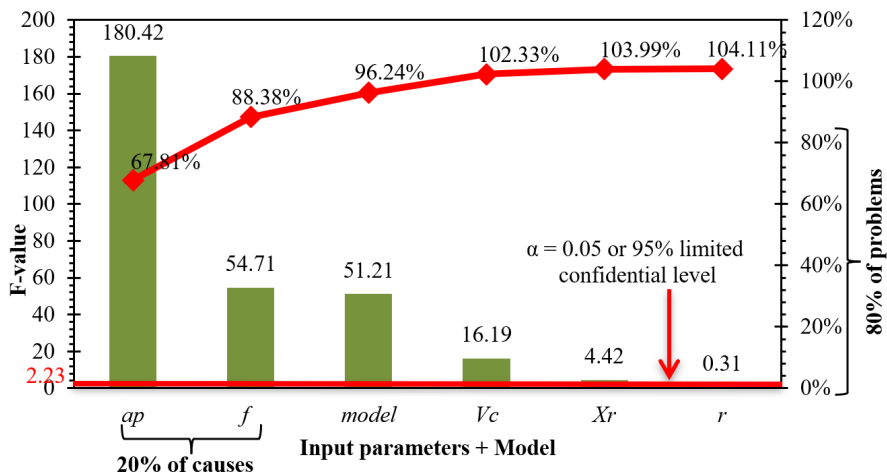


Fig. 3. Pareto chart of  $F_Z$

### 3.1.3. Cutting power ( $P_C$ )

Cutting power is a vital factor in polymer machining, but due to the distinct properties of polymers compared to metals, it is necessary to select cutting conditions that are tailored to these materials. As shown by Fig. 4, the depth of cut ( $ap$ ), the feed rate ( $f$ ), and the cutting speed ( $V_C$ ) are the most significant factors

for cutting power. Increasing  $ap$  and  $f$  systematically increases  $P_c$ . The depth of cut has the greatest influence on  $P_c$  (67.81%), followed by the feed rate (20.57%) and the cutting speed (6.09%). The effect of the principal cutting edge angle ( $X_r$ ) and the nose radius ( $r_\epsilon$ ) is negligible, despite the larger variation in  $X_r$  compared to  $r_\epsilon$ . The results from the Pareto analysis of  $P_c$  perfectly match the conclusions found by Chabbi et al. [7, 8]. Additionally, the results of the ANOVA analysis of  $P_c$  conducted by Paulo Davim in 2010 [25] during the turning of PEEK, PEEK CF30, and PEEK GF30 materials are in agreement with our results.

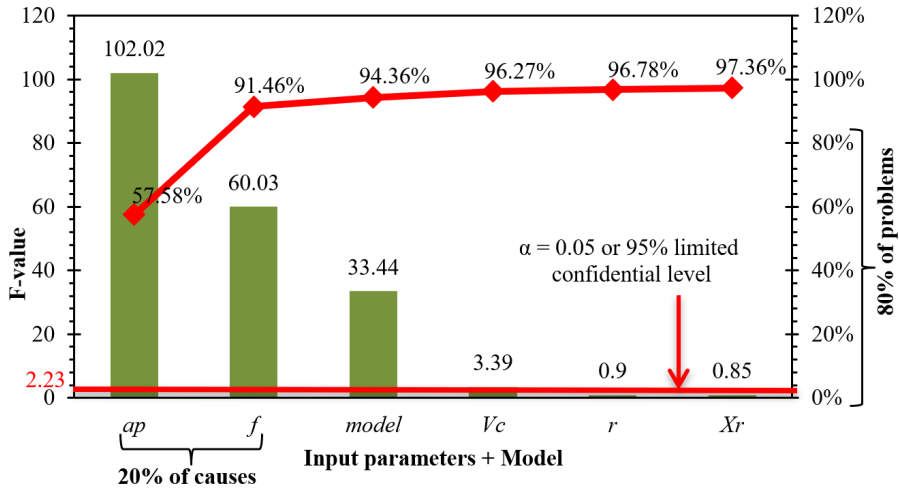
Fig. 4. Pareto chart of  $P_c$ 

### 3.1.4. Material removal rate ( $MRR$ )

Material removal rate ( $MRR$ ) is a crucial metric measuring the amount of material removed during machining per unit of time. For polymers, it is essential to maintain an appropriate  $MRR$  in order to avoid thermal deformation of the workpiece and excessive heat generation during the operation. In this case study, Fig. 5 presents the Pareto analysis of  $MRR$  during the turning POM-C.

The primary parameters influencing POM-C productivity are the depth of cut ( $ap$ ) and the feed rate ( $f$ ), contributing 57.58% and 33.88%, respectively. Cutting speed ( $V_c$ ) is less important and contributes only 1.91%. On the other hand, the main cutting edge angle ( $X_r$ ) and nose radius ( $r_\epsilon$ ) are the least important as their contribution is below the limited confidentiality level (2.2%). Therefore, these two factors have no significant impact on productivity. The Pareto analysis results for  $MRR$  are consistent with the ANOVA results performed by Chabbi et al. [7, 8] when turning the same plastic.

In summary, the cutting tool parameters  $X_r$  and  $r_\epsilon$  significantly impact only the first surface quality parameter,  $Ra$ . The feed rate is the most important independent

Fig. 5. Pareto chart of  $MRR$ 

variable that affects surface roughness, while the other factors ( $V_c$  and  $ap$ ) have an insignificant impact. On the contrary, the classic cutting parameters ( $V_c$ ,  $f$ , and  $ap$ ) have a significant effect on all three responses ( $F_z$ ,  $P_c$ , and  $MRR$ ). In this case, the depth of cut is the most important factor, followed by the feed rate and the cutting speed, each with a different contribution.

### 3.2. RSM-based Modeling

Response surface methodology (RSM) is a simple statistical method that allows generating a mathematical equation describing the relationship between a response variable  $Y$  (dependent variable) and several independent variables  $X_i$  ( $X_1, X_2, \dots, X_n$ ) [26–30]. In this study, multiple linear regression was used to create four output models ( $Ra$ ,  $F_z$ ,  $P_c$ , and  $MRR$ ) based on input factors ( $V_c$ ,  $f$ ,  $ap$ ,  $r_\epsilon$ , and  $X_r$ ). According to Mía et al. [31], the linear regression is often used to model machining when multiple attributes are simultaneously dominant. In such cases, a first-order linear model is generally sufficient. This method (RSM) is of great importance and widely used in design of experiments (DOE) to develop an empirical statistical model relating factors to a response [32–34]. The modeling using RSM is widely employed by numerous researchers in various fields, such as turning [35], drilling [36], milling [37], friction stir processing (FSP) [38], and many others.

The arithmetic surface roughness model ( $Ra$ ) is obtained from the multiple linear regression method and can be described by Eq. (3).

$$R_a = 4.024 - 0.00273V_c + 14.88f - 0.0531ap - 3.363r_\epsilon - 0.01550X_r, \quad (3)$$

$$(R_{Ra}^2 = 0.9672 = 96.72\%).$$

The determination coefficient ( $R_{Ra}^2$ ) of this model is very close to +1 ( $R_{Ra}^2 = 0.9672$ ), indicating that Eq. (3) is considered significant. Thus, this correlation explains 96.72% of the variations in the level of  $Ra$  roughness, with the remaining 3.28% unexplained. The value of the adjusted determination coefficient for  $Ra$  roughness is  $R_{adj}^2 = 0.9508$ , while the probability value is less than 0.05 ( $P < 0.05$ ). These results demonstrate a very good correlation between the experimental data and the model results. Figure 2 also shows that the Fisher test value is 58.99, which means that the portion of the variance of the surface roughness  $Ra$  explained by Eq. (3) is 58.99 times greater than the portion of the variance that remains unexplained.

The first-order model of the cutting force  $F_Z$  can be obtained using the same regression technique, as described by Eq. (4).

$$F_Z = -7.93 - 0.0776V_c + 256.6f + 26.48ap + 0.60r_\varepsilon - 0.0930X_r, \quad (4)$$

$$(R_{F_Z}^2 = 0.9861 = 98.61\%).$$

The values of the determination coefficient  $R^2$  and the adjusted determination coefficient  $R_{adj}^2$  for the principal cutting force  $F_Z$  have been calculated and are respectively equal to 0.9861 and 0.9792. Furthermore, the probability value  $P$  is strictly less than 0.05, indicating that the linear model is statistically significant. These results demonstrate a strong correlation between the experimental data and the results obtained by this model.

The first-order model of the cutting power  $P_c$  was obtained using the linear regression method, with the formula given by Eq. (5). The values of the coefficient  $R_{P_c}^2$  and the adjusted coefficient  $R_{adj}^2$  have been calculated and are respectively 0.9624 and 0.9436. Furthermore, the Fisher test ( $F$ ) for the model yields a value of  $F = 51.21$  and the probability ( $P$ ) associated with this test is less than 0.05. These results indicate that the mathematical model of the cutting power is well-correlated with the experimental data.

$$P_c = -217.7 + 0.524V_c + 1065f + 131.11ap - 24.2r_\varepsilon - 1.224X_r, \quad (5)$$

$$(R_{P_c}^2 = 0.9624 = 96.24\%).$$

Linear regression has provided the mathematical equation linking the material removal rate ( $MRR$ ) to the five input variables, as given by Eq. (6).

$$MRR = -86.7 + 0.1144V_c + 533.1f + 47.10ap - 19.8r_\varepsilon - 0.256X_r, \quad (6)$$

$$(R_{MRR}^2 = 0.9436 = 94.36\%).$$

In Fig. 6, a comparison is presented between the experimental data of the responses ( $Ra$ ,  $F_Z$ , and  $P_c$ ) and the results predicted by the three multiple regression mathematical models. This comparison confirms the strong correlation between the experimental data and the values generated by the regression models, as all

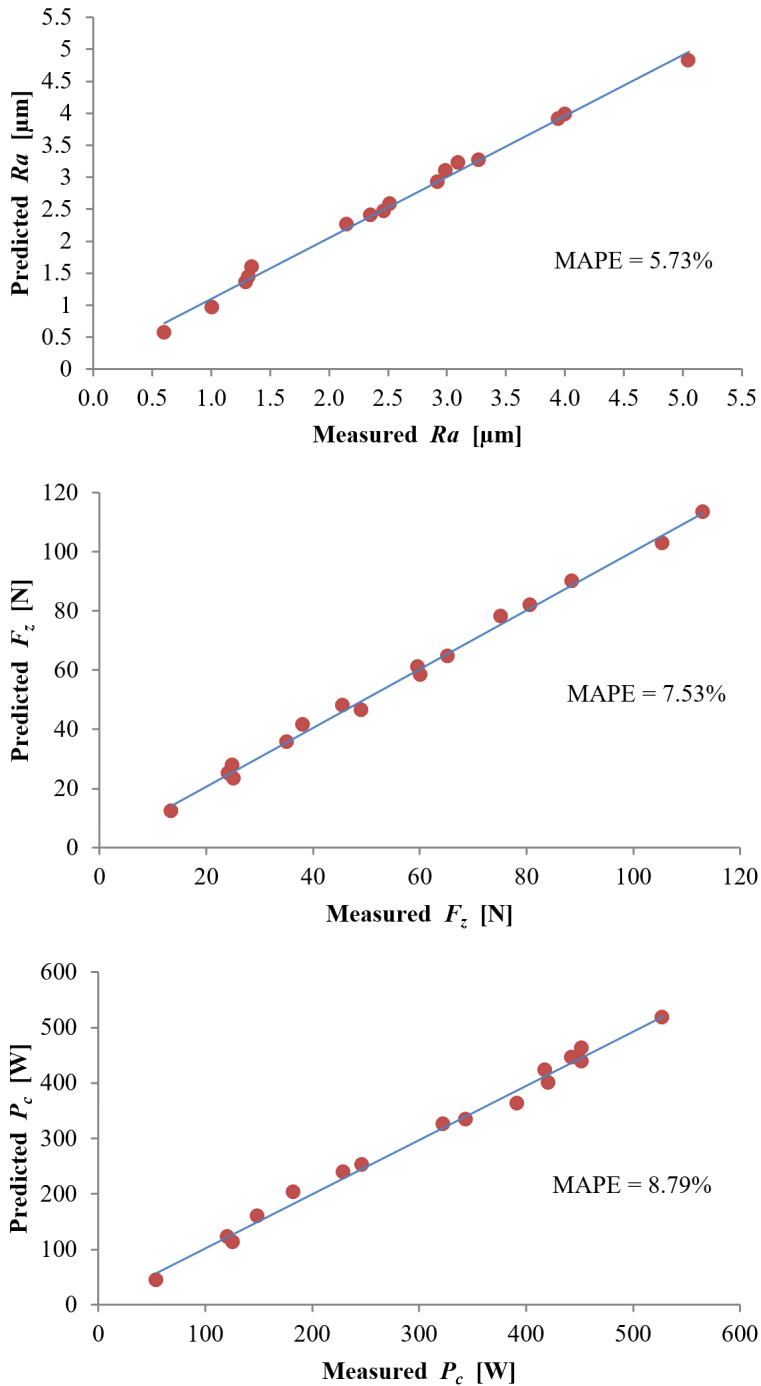


Fig. 6. Comparison between experimental data and predicted results of the three responses ( $R_a$ ,  $F_z$ , and  $P_c$ )

the points are very close to each other. Additionally, the red points represent the experimental values, while the blue lines represent the values predicted by the models. Indeed, one can observe that the points and the lines almost perfectly overlap, indicating a strong correlation between the experimental data and the values predicted. Therefore, the three mathematical models can be used to predict the values of the three output parameters ( $Ra$ ,  $F_Z$ , and  $P_c$ ) within the specified range of turning parameters (Table 2).

### 3.3. 3D response surfaces analysis

To enhance the clarity of response surface representation in this paper without altering relevant information, three-dimensional (3D) plots were created for these surfaces. These plots were based on the most influential factors, with other operational variables held constant at the central level within the factor's variation domain. Design Expert 11 software was used to obtain the 3D response surfaces. Figs 7 to 9 illustrate the 3D response surface plots of the three models (3, 4, and 5) as a function of the interaction of the most significant control parameters. The interactions can be interpreted as follows:

- Fig. 7a shows the effect of the two most significant factors, namely feed rate ( $f$ ) and nose radius ( $r_\epsilon$ ), on the dependent variable  $Ra$  (see also Fig. 2). We observe that increasing  $f$  leads to an increase in  $Ra$  roughness, while increasing the nose radius ( $r_\epsilon$ ) results in a decrease in  $Ra$ . Therefore, to obtain a better surface quality of POM-C, it is recommended to choose a low feed rate ( $f$ ) and a large tool nose radius ( $r_\epsilon$ ).
- Fig. 7b presents the effect of the interaction between the feed rate and the primary cutting edge angle ( $X_r$ ) on the  $Ra$  response. We can observe that increasing  $X_r$  leads to improved surface quality (decrease in  $Ra$ ) when the feed rate  $f$  is low, while at high values of  $f$ , the effect of  $X_r$  is less significant. In other words, to obtain a better surface quality of POM-C, it is recommended to work with a low feed rate and a high principal cutting edge angle.
- Fig. 7c shows how the interaction of  $f \times V_c$  affects the response variable  $Ra$ . It can be observed that the feed rate has a greater influence than the cutting speed. However, to obtain a good surface quality, it is recommended to use a high cutting speed.
- Fig. 8a illustrates how the interaction  $ap \times f$  affects the cutting force  $F_Z$ . One can observe that increasing the depth of cut leads to increased cutting force, with the effect being accelerated at higher feed rates.
- Fig. 8b illustrates how the interaction between the depth of cut ( $ap$ ) and the cutting speed ( $V_c$ ) affects the cutting force. It can be seen that, in order to obtain a low cutting force, it is recommended to use a low depth of cut and a high cutting speed.

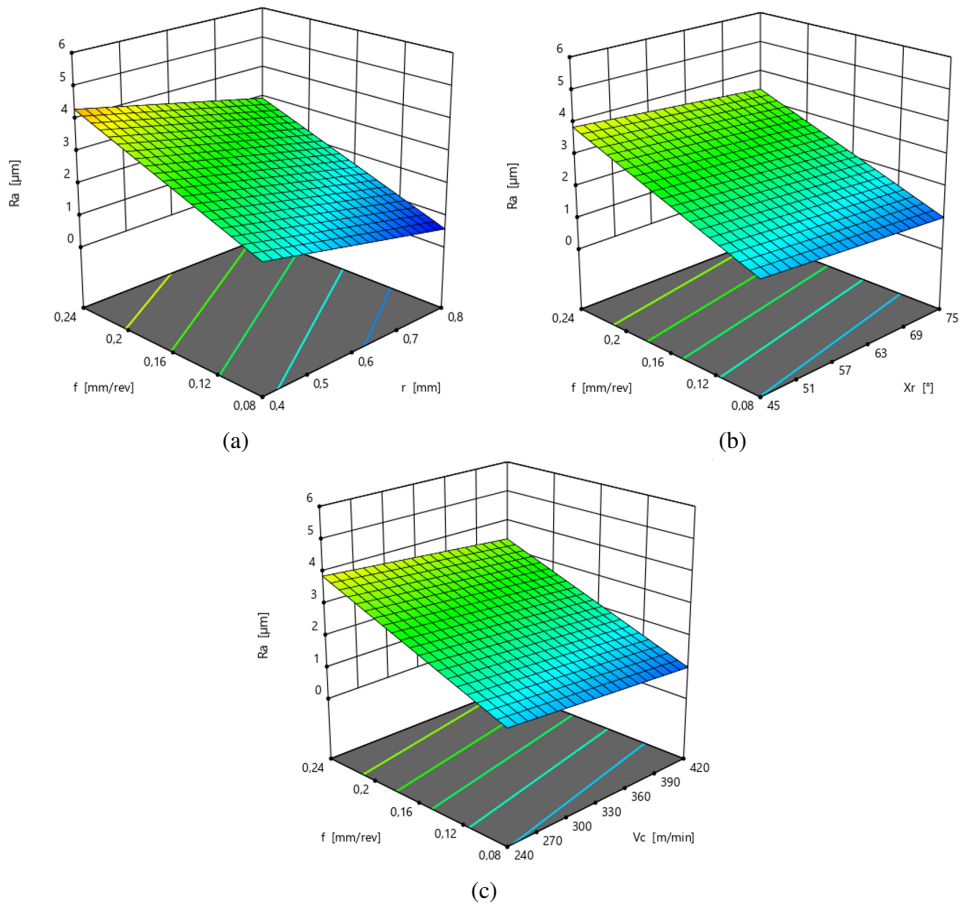


Fig. 7. 3D response surfaces of  $R_a$  roughness as a function of the most significant factors

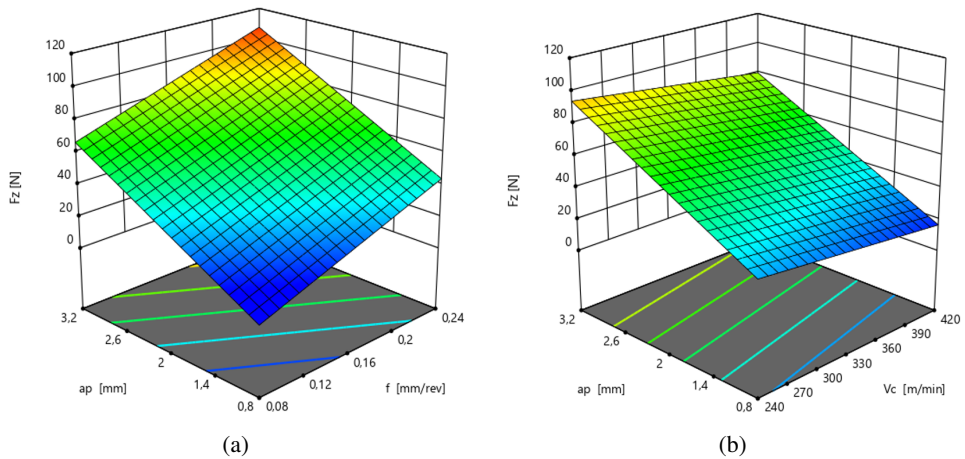


Fig. 8. 3D response surfaces of cutting force ( $F_z$ ) as a function of the most significant factors

- Figs 9a and 9b, the effects of the interactions  $ap \times f$  and  $ap \times V_c$  on the cutting power  $P_c$ , are illustrated, respectively. The graphs exhibit a marked similarity between the variation in cutting force and cutting power. This similarity can be explained by calculation of the cutting power from the cutting force and a fixed cutting speed of 60 m/min.
- For the chosen range of values for turning POM-C polymer, it is consistently observed that the feed rate exerts a positive influence on all three studied responses ( $Ra$ ,  $F_Z$ , and  $P_c$ ).

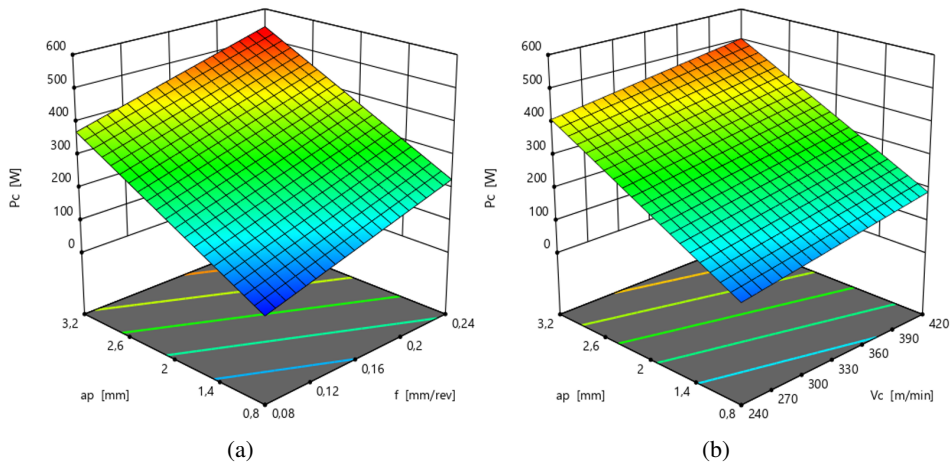


Fig. 9. 3D response surfaces of the  $P_c$  as a function of the most significant factors

### 3.4. Validation tests

To verify the quality, accuracy, and performance of the RSM-developed models, four additional experimental validation tests were carried out. The cutting conditions were chosen within the ranges outlined in Table 2. The results, which are presented in Table 4, indicate that the absolute prediction error (APE) values range from 2.61% to 14.39% for  $Ra$ , 4.66% to 19.13% for  $F_Z$ , 4.95% to 21.18% for  $P_c$ , and 7.21% to 22.82% for  $MRR$ . These results confirm the ability of the models to predict new outcomes during the turning of POM-C.

### 3.5. Optimization of cutting parameters

Optimizing cutting parameters is crucial in material removal machining, as it plays a key role in enhancing part quality, increases productivity, and reduces production costs. To achieve these objectives, different optimization methods are available. For instance, metaheuristic algorithms have emerged as effective optimization techniques for machining conditions. Some of the commonly used algorithms are the genetic algorithm (GA), the simulated annealing (SA), and the particle swarm

Table 4. Results of confirmatory testing

No.	$V_c$ [m/min]	$f$ [mm/rev]	$ap$ [mm]	$r_\varepsilon$ [mm]	$X_r$ [°]	Experimental results	Predicted results	APE [%]
(a) Surface roughness $Ra$ [ $\mu\text{m}$ ]								
1	320	0.16	1	0.4	75	2.59	2.97	12.79
2	380	0.18	2	0.8	75	1.73	1.70	1.76
3	280	0.18	1.2	0.4	45	3.72	3.83	2.87
4	400	0.22	0.8	0.8	45	2.2	2.57	14.39
(b) Cutting force $F_Z$ [N]								
1	320	0.16	1	0.4	75	30.55	28.04	8.95
2	380	0.18	2	0.8	75	63.65	55.24	15.22
3	280	0.18	1.2	0.4	45	35.88	44.37	19.13
4	400	0.22	0.8	0.8	45	36.59	34.96	4.66
(c) Cutting power $P_c$ [W]								
1	320	0.16	1	0.4	75	162.93	150.01	8.61
2	380	0.18	2	0.8	75	380.11	324.18	17.25
3	280	0.18	1.2	0.4	45	168.1	213.29	21.18
4	400	0.22	0.8	0.8	45	243.93	256.64	4.95
(d) Material removal rate $MRR$ [ $\text{cm}^3/\text{min}$ ]								
1	320	0.16	1	0.4	75	51.2	55.184	7.21
2	380	0.18	2	0.8	75	136.8	111.89	22.26
3	280	0.18	1.2	0.4	45	60.48	78.37	22.82
4	400	0.22	0.8	0.8	45	70.4	86.662	18.76

optimization (PSO). The genetic algorithm is a highly effective search technique that emulates natural evolution [39].

The genetic algorithm is increasingly used in many engineering fields because it is easy to implement and effective in solving complex problems involving multiple input parameters [40–42]. The GA follows a basic cycle that can be adapted and improved to meet the specific requirements of optimization problems. The main steps of this cycle are as follows:

1. Generation of an initial population of possible individuals, represented by strings of genes.
2. Evaluating the fitness of each individual based on a defined performance measure for the problem.
3. Selection of the most successful individuals for reproduction.
4. Crossing the gene chains of selected individuals to create new individuals.
5. Introduction of random mutations to create diversity in the population.
6. Repetition of the selection, crossing, and mutation process over multiple generations until a satisfactory solution is found.

Genetic algorithm (GA) can be used to solve multi-objective optimization problems by simultaneously optimizing multiple performance criteria, known as “objectives”. In this case, the GA must be adapted to find a “Pareto frontier”, which represents all solutions that cannot be improved without degrading at least one of the objectives. According to Ganesan et al. [43].

To improve the machinability of POM-C turning, we divided our optimization into several sets of independent variables, namely  $(Ra, MRR)$ ,  $(F_Z, MRR)$ ,  $(Ra, P_c)$ , and  $(MRR, P_c)$ . We also performed a combinatorial optimization of three objectives:  $Ra$ ,  $F_Z$ , and  $MRR$ . The goal of these combinations is to maximize productivity ( $MRR$ ) while reducing the other response parameters. Equations (3) to (6) are used as objective functions. The multi-objective optimization problem can be formulated as follows: Determine the values of  $V_c$ ,  $f$ ,  $a_p$ ,  $r_\varepsilon$ , and  $X_r$  to minimize  $Ra$ ,  $F_Z$ ,  $P_c$  while maximizing  $MRR$ , subject to the following constraints:  $240 \leq V_c$  (m/min)  $\leq 420$ ;  $0.08 \leq f$  (mm/rev)  $\leq 0.24$ ;  $0.8 \leq a_p$  (mm)  $\leq 3.2$ ;  $r_\varepsilon$  (mm) = 0.4 or 0.8, and  $X_r$  ( $^\circ$ ) = 45 or 75.

### 3.5.1. Optimization of $Ra$ and $MRR$

The Pareto front serves as a multi-objective analysis method, facilitating the identification of optimal solutions that simultaneously satisfy multiple criteria by establishing a compromise among them. In our study, we identified 70 optimal solutions, represented by violet stars, within the considered range. From these, we selected the three best solutions among them. Fig. 10 and Table 5 present the results of the Pareto front for the  $Ra$  and  $MRR$  pair. This Pareto front illustrates a proportional relationship between surface roughness and material removal rate for different combinations of cutting parameters. In other words, as the  $MRR$  increases, the surface roughness also increases. This suggests that the faster you remove material, the rougher the surface of the machined part will be. However, it is important to note that this proportional relationship is not always linear and

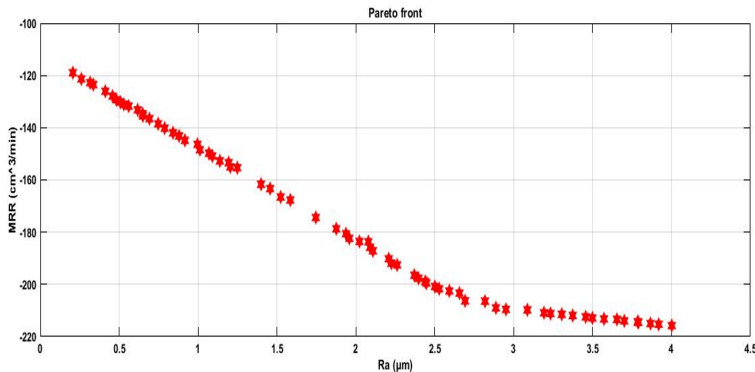


Fig. 10. Optimization of  $Ra$  and  $MRR$  pair by GA

may vary depending on the cutting parameters used. In this case, the optimal cutting parameters to achieve a surface roughness of  $0.62 \mu\text{m}$  and an  $MRR$  of  $133.15 \text{ cm}^3/\text{min}$  are  $V_c = 410 \text{ m/min}$ ,  $f = 0.11 \text{ mm/rev}$ ,  $ap = 3.17 \text{ mm}$ ,  $r_\epsilon = 0.8 \text{ mm}$ , and  $X_r = 75^\circ$ .

Table 5. Results of GA optimization for  $Ra$  and  $MRR$ 

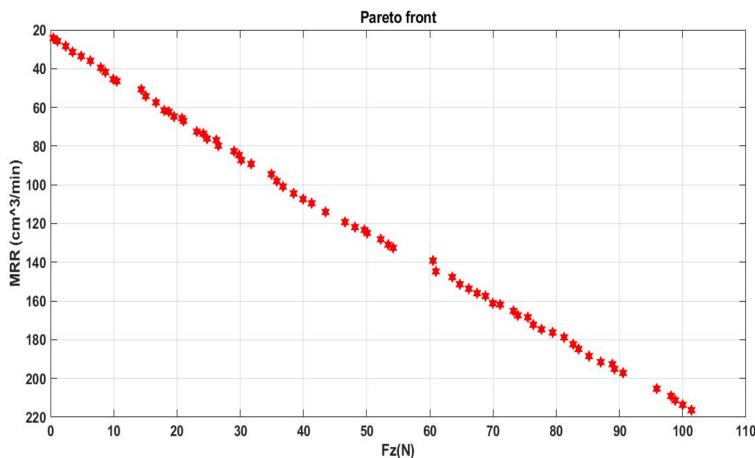
No.	$V_c$ [m/min]	$f$ [mm/rev]	$ap$ [mm]	$r_\epsilon$ [mm]	$X_r$ [ $^\circ$ ]	$Ra$ [ $\mu\text{m}$ ]	$MRR$ [ $\text{cm}^3/\text{min}$ ]
1	409.76	0.11	3.17	0.80	75.00	0.62	133.15
2	410.23	0.11	3.19	0.80	75.00	0.64	134.62
3	410.18	0.11	3.19	0.80	75.00	0.65	135.46

### 3.5.2. Optimization of $F_Z$ and $MRR$

The cutting force plays a crucial role in the machining process. To minimize expenses, the manufacturing sector is dedicating efforts to the exploration of minimal cutting forces [44]. Table 6 and Fig. 11 show the results of the independent

Table 6. Optimization results of  $F_Z$  and  $MRR$  using GA

No.	$V_c$ [m/min]	$f$ [mm/rev]	$ap$ [mm]	$r_\epsilon$ [mm]	$X_r$ [ $^\circ$ ]	$F_Z$ [N]	$MRR$ [ $\text{cm}^3/\text{min}$ ]
1	410.66	0.12	1.10	0.40	45.00	14.37	50.77
2	412.30	0.14	0.94	0.40	45.00	15.07	54.19
3	414.80	0.13	1.06	0.40	45.00	16.68	57.45

Fig. 11. Optimization of  $F_Z$  and  $MRR$  couple by the GA

variable optimization for tangential force ( $F_Z$ ) and material removal rate ( $MRR$ ) when machining POM-C. In this study, tangential force and  $MRR$  are positively correlated, meaning that when tangential force increases, so does  $MRR$ . However, it is important to note that this relationship is not always linear. The optimal cutting parameters to achieve a cutting force of 14.37 N and an  $MRR$  of 50.77 cm<sup>3</sup>/min are as follows:  $V_c = 410$  m/min,  $f = 0.12$  mm/rev,  $ap = 1.1$  mm,  $r_\varepsilon = 0.4$  mm, and  $X_r = 45^\circ$ .

### 3.5.3. Optimization of $Ra$ and $P_c$

Table 7 and Fig. 12 show the torque optimization results of roughness ( $Ra$ ) and cutting power ( $P_c$ ). In our case, as cutting power increases, surface roughness decreases because there is less contact between the tool and the workpiece. This allows the material to be removed more efficiently, resulting in a smoother surface. The optimal cutting parameters to achieve a roughness of 0.6  $\mu\text{m}$  and a cutting power of 121.22 W are as follows: a cutting speed ( $V_c$ ) of 320 m/min, a feed rate ( $f$ ) of 0.08 mm/rev, a depth of cut ( $ap$ ) of 0.8 mm, a nose radius ( $r_\varepsilon$ ) of 0.8 mm, and a main cutting edge angle ( $X_r$ ) of  $75^\circ$ .

Table 7. Results of Pareto-optimal solutions for  $Ra$  and  $P_c$

No.	$V_c$ [m/min]	$f$ [mm/rev]	$ap$ [mm]	$r_\varepsilon$ [mm]	$X_r$ [ $^\circ$ ]	$Ra$ [ $\mu\text{m}$ ]	$P_c$ [W]
1	320.07	0.08	0.81	0.80	75.00	0.60	121.22
2	305.93	0.08	0.87	0.80	75.00	0.63	119.96
3	310.75	0.08	0.81	0.80	75.00	0.64	115.99

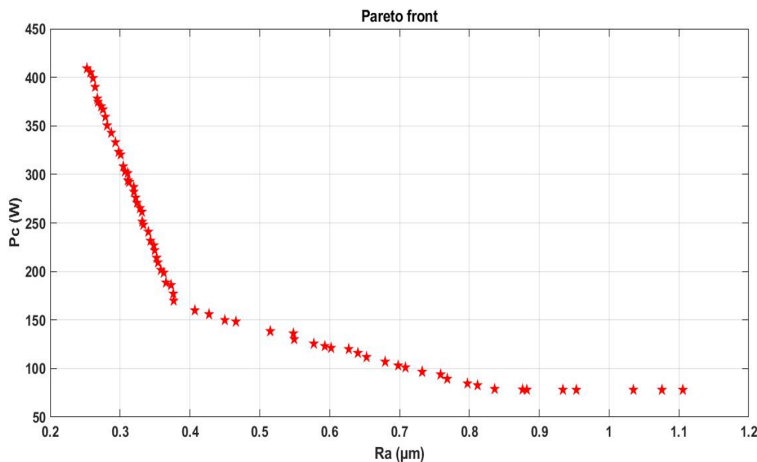


Fig. 12. Graph of the Pareto-optimal solutions of  $Ra$  and  $P_c$

### 3.5.4. Optimization of 3 objectives

Table 8 displays the optimization results for the three response criteria ( $Ra$ ,  $F_Z$ , and  $MRR$ ) concerning the five factors ( $V_c$ ,  $f$ ,  $ap$ ,  $r_\epsilon$ , and  $X_r$ ) using the genetic algorithm. It is evident that as surface roughness ( $Ra$ ) increases, cutting force ( $F_Z$ ) also increases, while  $MRR$  decreases. Therefore, there exists an inverse proportional relationship between  $Ra$ ,  $F_Z$ , and  $MRR$ . To obtain optimal cutting parameters, it is recommended to use  $V_c = 370$  m/min,  $f = 0.09$  mm/rev,  $ap = 2.38$  mm,  $r_\epsilon = 0.8$  mm, and  $X_r = 75^\circ$ , which yield the following values for the dependent variables:  $Ra = 0.66$   $\mu\text{m}$ ,  $F_Z = 42.1$  N, and  $MRR = 80.9$   $\text{cm}^3/\text{min}$ .

Table 8. Results of optimization of three criteria ( $Ra$ ,  $F_Z$ , and  $MRR$ ) using the GA

No.	$V_c$ [m/min]	$f$ [mm/rev]	$ap$ [mm]	$r_\epsilon$ [mm]	$X_r$ [ $^\circ$ ]	$Ra$ [ $\mu\text{m}$ ]	$F_Z$ [N]	$MRR$ [ $\text{cm}^3/\text{min}$ ]
1	370.80	0.09	2.38	0.80	75.00	0.66	42.10	80.90
2	376.07	0.09	1.33	0.80	75.00	0.84	16.19	36.86
3	372.44	0.10	2.28	0.80	75.00	0.93	42.43	83.44
4	360.66	0.10	1.92	0.80	75.00	0.99	34.28	65.94
5	362.07	0.10	1.53	0.80	75.00	1.02	23.34	46.97
6	354.54	0.09	1.28	0.80	75.00	1.07	16.03	32.23
7	357.15	0.10	1.67	0.80	75.00	1.09	27.90	54.22
8	357.46	0.11	1.18	0.80	75.00	1.16	18.19	37.10
9	364.60	0.11	1.21	0.80	75.00	1.20	19.33	41.26
10	364.55	0.11	1.78	0.80	75.00	1.27	33.88	67.81

## 4. Conclusions

In conclusion, this study utilized Pareto analysis, linear regression, and genetic algorithm to assess the impact of five input parameters ( $V_c$ ,  $f$ ,  $ap$ ,  $r_\epsilon$ , and  $X_r$ ) on four output parameters ( $Ra$ ,  $F_Z$ ,  $P_c$ , and  $MRR$ ) during the turning of POM-C thermoplastic material. The findings have led to the following key insights:

- Pareto analysis indicated that the feed rate had the most significant influence, contributing 58.05% to the  $Ra$  parameter. Additionally, the nose radius of the cutting tool and the main cutting edge angle also had notable impacts, contributing 32.25% and 3.86%, respectively. To enhance the surface quality of POM-C, it is recommended to opt for a lower feed rate and a larger nose radius.
- Traditional factors like  $V_c$ ,  $f$ , and  $ap$  significantly affected the three dependent variables ( $F_Z$ ,  $P_c$ , and  $MRR$ ). The depth of cut emerged as the most

influential factor, followed by  $f$  and  $V_c$ . However, their contributions varied depending on the specific response under consideration.

- The linear regression models developed for  $Ra$ ,  $F_Z$ ,  $P_c$ , and  $MRR$  demonstrated robust fits with the experimental data, with coefficients of determination ( $R^2$ ) reaching 96.72%, 98.61%, 96.24%, and 94.36%, respectively. These models offer practical utility in predicting output parameter values based on chosen cutting parameters.
- The optimal cutting parameters, identified to minimize  $Ra$  and  $F_Z$  while maximizing  $MRR$ , are as follows:  $V_c = 250$  m/min,  $f = 0.1$  mm/rev,  $ap = 0.9$  mm,  $r_\epsilon = 0.4$  mm, and  $X_r = 75^\circ$ . These settings yielded results of  $0.66 \mu\text{m}$  for  $Ra$ ,  $42.1$  N for  $F_Z$ , and  $80.9 \text{ cm}^3/\text{min}$  for  $MRR$ . The optimization approach employing GA has proven to be promising and effective in determining optimal cutting parameters for enhanced productivity and improved surface quality.
- The findings of this study provide valuable insights and pave the way for future research, enabling further examination of interactions between factors and responses. Potential extensions include exploring the impact of coated cutting tools, minimum quantity lubrication (MQL), or lubricant type on parameters such as cutting time, cutting energy, and specific cutting energy. Additionally, the study can encompass diverse materials or machining techniques for performance comparisons and optimization.

### Acknowledgements

This work was carried out in the LIMMaS laboratory (Tissemsilt University, Algeria) in collaboration with LMS laboratory (Guelma University, Algeria). The authors would like to thank the “Metal Cutting Research Group” of the LMS laboratory, 8 May 1945 University, Guelma, Algeria.

The present research was received funding from the General Directorate of Scientific Research and Technological Development (DGRSDT) under the PRFU research project A11N01UN380120220002.

### References

- [1] A.I. Alateyah, Y. El-Taybany, S. El-Sanabary, W.H. El-Garaihy, and H. Kouta. Experimental investigation and optimization of turning polymers using RSM, GA, hybrid FFD-GA, and MOGA methods. *Polymers*, 14(17):3585, 2022. doi: [10.3390/polym14173585](https://doi.org/10.3390/polym14173585).
- [2] M. Madić, D. Marković, and M. Radovanović. Mathematical modeling and optimization of surface roughness in turning of polyamide based on artificial neural network. *MECHANIKA*, 18(5):574–581, 2012. doi: [10.5755/j01.mech.18.5.2701](https://doi.org/10.5755/j01.mech.18.5.2701).
- [3] K. Palanikumar. Modeling and analysis for surface roughness in machining glass fibre reinforced plastics using response surface methodology. *Materials and Design*, 28:2611–2618, 2007a. doi: [10.1016/j.matdes.2006.10.001](https://doi.org/10.1016/j.matdes.2006.10.001).

- [4] K. Palanikumar and J. Paulo Davim. Mathematical model to predict tool wear on the machining of glass fibre reinforced plastic composites. *Materials and Design* 28:2008–2014, 2007b. doi: [10.1016/j.matdes.2006.06.018](https://doi.org/10.1016/j.matdes.2006.06.018).
- [5] V.N. Gaitonde, S.R. Karnik, F. Mata, and J. Paulo Davim. Taguchi approach for achieving better machinability in unreinforced and reinforced polyamides. *Journal of Reinforced Plastics and Composites*, 27(9):909–924, 2008. doi: [10.1177/0731684407085875](https://doi.org/10.1177/0731684407085875).
- [6] F. Mata, P. Reis, and J. Paulo Davim. Physical cutting model of polyamide composites (PA66 GF30). *Materials Science Forum*, 514-516:643–647, 2006. doi: [10.4028/www.scientific.net/MSF.514-516.643](https://doi.org/10.4028/www.scientific.net/MSF.514-516.643).
- [7] A. Chabbi, M.A. Yallese, M. Nouioua, I. Meddour, T. Mabrouki, and F. Girardin. Modeling and optimization of turning process parameters during the cutting of polymer (POM C) based on RSM, ANN, and DF methods. *International Journal of Advanced Manufacturing Technology*, 91:2267–2290, 2017a. doi: [10.1007/s00170-016-9858-8](https://doi.org/10.1007/s00170-016-9858-8).
- [8] A. Chabbi, M.A. Yallese, M. Nouioua, I. Meddour, T. Mabrouki, and F. Girardin. Predictive modeling and multi-response optimization of technological parameters in turning of Polyoxymethylene polymer (POM C) using RSM and desirability function. *Measurement*, 95:99–115, 2017b. doi: [10.1016/j.measurement.2016.09.043](https://doi.org/10.1016/j.measurement.2016.09.043).
- [9] M. Alauddin, I.A. Choudhury, M.A. El Baradie, and M.S.J. Hashmi. Plastics and their machining: a review. *Journal of Materials Processing Technology*, 54:40–46, 1995. doi: [10.1016/0924-0136\(95\)01917-0](https://doi.org/10.1016/0924-0136(95)01917-0).
- [10] J. Paulo Davim and F. Mata. Optimisation of surface roughness on turning fibre-reinforced plastics (FRPs) with diamond cutting tools. *International Journal of Advanced Manufacturing Technology*, 26:319–323, 2005. doi: [10.1007/s00170-003-2006-2](https://doi.org/10.1007/s00170-003-2006-2).
- [11] J. Paulo Davim and F. Mata. A comparative evaluation of the turning of reinforced and unreinforced polyamide. *International Journal of Advanced Manufacturing Technology*, 33:911–914, 2007. doi: [10.1007/s00170-006-0520-8](https://doi.org/10.1007/s00170-006-0520-8).
- [12] J. Paulo Davim, L.R. Silva, A. Festas, and A.M. Abrão. Machinability study on precision turning of PA66 polyamide with and without glass fiber reinforcing. *Materials and Design*, 30:228–234, 2009. doi: [10.1016/j.matdes.2008.05.003](https://doi.org/10.1016/j.matdes.2008.05.003).
- [13] K. Palanikumar, T. Rajasekaran, and B. Latha. Fuzzy rule-based modeling of machining parameters for surface roughness in turning carbon particle-reinforced polyamide. *Journal of Thermoplastic Composite Materials*, 28(10):1387–1405, 2015. doi: [10.1177/0892705713513282](https://doi.org/10.1177/0892705713513282).
- [14] N. Hamlaoui, S. Azzouz, K. Chaoui, Z. Azari, and M.A. Yallese. Machining of tough polyethylene pipe material: surface roughness and cutting temperature optimization. *International Journal of Advanced Manufacturing Technology*, 92:2231–2245, 2017. doi: [10.1007/s00170-017-0275-4](https://doi.org/10.1007/s00170-017-0275-4).
- [15] F.M. Cabrera, D. Fuentes, I. Hanafi, A. Khamlichi, and A. Jabbouri. Multi-criteria optimization using Taguchi and grey relational analysis in CNC Turning of PEEK CF30. *Journal of Thermoplastic Composite Materials*. 25(11):101–114, 2012. doi: [10.1177/0892705711405248](https://doi.org/10.1177/0892705711405248).
- [16] F.M. Cabrera, E. Beamud, and I. Hanafi. Fuzzy logic-based modeling of surface roughness parameters for CNC turning of PEEK CF30 by TiN-Coated cutting tools. *Journal of Thermoplastic Composite Materials*, 24(3):399–413, 2010. doi: [10.1177/0892705710391562](https://doi.org/10.1177/0892705710391562).
- [17] H. Akkuş and H. Yaka. Optimization of cutting parameters in turning of titanium alloy (Grade 5) by analyzing surface roughness, tool wear and energy consumption. *Experimental Techniques*, 46:945–956, 2022. doi: [10.1007/s40799-021-00525-6](https://doi.org/10.1007/s40799-021-00525-6).
- [18] G. Özden, F. Mata, and M.Ö. Öteyaka. Artificial neural network modeling for prediction of cutting forces in turning unreinforced and reinforced polyamide. *Journal of Thermoplastic Composite Materials*, 34(3):353–363, 2019. doi: [10.1177/089270571984](https://doi.org/10.1177/089270571984).

- [19] V.N. Gaitonde, S.R. Karnik, F. Mata, and J. Paulo Davim. Modeling and analysis of machinability characteristics in PA6 and PA66 GF30 polyamides through artificial neural network. *Journal of Thermoplastic Composite Materials*, 23(3):313–336, 2010. doi: [10.1177/0892705709349319](https://doi.org/10.1177/0892705709349319).
- [20] N. Baroiu, G.A. Costin, V.G. Teodor, D. Nedelcu, and V. Tabacaru. Prediction of surface roughness in drilling of polymers using a geometrical model and artificial neural networks. *Materiale Plastice* 57(3):160–173, 2020. doi: [10.37358/MP.20.3.5390](https://doi.org/10.37358/MP.20.3.5390).
- [21] V. Tabacaru. Artificial neural networks applied to prediction of surface roughness in dry drilling of some polymers. *IOP Conf. Ser.: Mater. Sci. Eng.*, 916 012117, 2020. doi: [10.1088/1757-899X/916/1/012117](https://doi.org/10.1088/1757-899X/916/1/012117).
- [22] A. Zerti, M.A. Yallese, O. Zerti, M. Nouioua, and R. Khettabi. Prediction of machining performance using RSM and ANN models in hard turning of martensitic stainless steel AISI 420. *Proceedings of the Institution of Mechanical Engineers, Part C: Journal of Mechanical Engineering Science*, 233(13):4439–4462, 2019a. doi: [10.1177/0954406218820557](https://doi.org/10.1177/0954406218820557).
- [23] A. Zerti, M.A. Yallese, I. Meddour, S. Belhadi, A. Haddad, and T. Mabrouki. Modeling and multi-objective optimization for minimizing surface roughness, cutting force, and power, and maximizing productivity for tempered stainless steel AISI 420 in turning operations. *International Journal of Advanced Manufacturing Technology*, 102:135–157, 2019b. doi: [10.1007/s00170-018-2984-8](https://doi.org/10.1007/s00170-018-2984-8).
- [24] A. Zaidi, S. Boucherit, M.A. Yallese, S. Belhadi, and M. Kaddeche. RSM modeling and multi-objective optimization of turning parameters for polyamide PA66 using PCA and PCA coupled with TOPSIS. *MECHANIKA*, 28(6):499–508, 2022. doi: [10.5755/j02.mech.30394](https://doi.org/10.5755/j02.mech.30394).
- [25] J. Paul Davim, F. Mata, V.N. Gaitonde, and S.R. Karnik. Machinability evaluation in unreinforced and reinforced PEEK composites using response surface models. *Journal of Thermoplastic Composite Materials*, 23(1):5–18, 2010. doi: [10.1177/0892705708093503](https://doi.org/10.1177/0892705708093503).
- [26] K. Safi, M.A. Yallese, S. Belhadi, T. Mabrouki, and A. Laouissi. Tool wear, 3D surface topography, and comparative analysis of GRA, MOORA, DEAR, and WASPAS optimization techniques in turning of cold work tool steel. *International Journal of Advanced Manufacturing Technology*, 121:701–721, 2022. doi: [10.1007/s00170-022-09326-6](https://doi.org/10.1007/s00170-022-09326-6).
- [27] M. Nouioua, A. Laouissi, V. Brahami, M.M. Blaoui, A. Hammoudi, and M.A. Yallese. Evaluation of: MOSSA, MOALO, MOVO and MOGWO algorithms in green machining to enhance the turning performances of X210Cr12 steel. *International Journal of Advanced Manufacturing Technology*, 120:2135–2150, 2022. doi: [10.1007/s00170-022-08897-8](https://doi.org/10.1007/s00170-022-08897-8).
- [28] R. Suresh, A.G. Joshi, and M. Manjaiah. Experimental investigation on tool wear in AISI H13 die steel turning using RSM and ANN methods. *Arabian Journal for Science and Engineering*, 46:2311–2325, 2021. doi: [10.1007/s13369-020-05038-9](https://doi.org/10.1007/s13369-020-05038-9).
- [29] B. Hamadi, M.A. Yallese, L. Boulanouar, A. Hammoudi, and M. Nouioua. Evaluation of the cutting performance of PVD, CVD and MTCVD carbide inserts in dry turning of AISI 4140 steel using RSM-based NAMDE optimization. *Journal of the Brazilian Society of Mechanical Sciences and Engineering*, 44:342, 2022. doi: [10.1007/s40430-022-03633-5](https://doi.org/10.1007/s40430-022-03633-5).
- [30] A. Hamdi, S.M. Merghache, and T. Aliouane. Effect of cutting variables on bearing area curve parameters (BAC-P) during hard turning process. *Archive Mechanical Engineering*, 67(1):73–95, 2020. doi: [10.24425/ame.2020.131684](https://doi.org/10.24425/ame.2020.131684).
- [31] M. Mia and N.R. Dhar. Modeling of surface roughness using RSM, FL and SA in dry hard turning. *Arabian Journal for Science and Engineering*, 43:1125–1136, 2018. doi: [10.1007/s13369-017-2754-1](https://doi.org/10.1007/s13369-017-2754-1).
- [32] P.B. Zaman and N.R. Dhar. Multi-objective optimization of double-jet MQL system parameters meant for enhancing the turning performance of Ti–6Al–4V Alloy. *Arabian Journal for Science and Engineering*, 45:9505–9526, 2020. doi: [10.1007/s13369-020-04806-x](https://doi.org/10.1007/s13369-020-04806-x).

- [33] N. Senthilkumar, T. Tamizharasan, and S. Gobikannan. Application of Response Surface Methodology and Firefly Algorithm for Optimizing Multiple Responses in Turning AISI 1045 Steel. *Arabian Journal for Science and Engineering*, 39:8015–8030, 2014. doi: [10.1007/s13369-014-1320-3](https://doi.org/10.1007/s13369-014-1320-3).
- [34] K. Noor, M.A. Siddiqui, and S.A. Iqbal. Multi-objective optimization of parameters in CNC turning of a hardened alloy steel roll by using response surface methodology. *Arabian Journal for Science and Engineering*, 48:3403–3423, 2023. doi: [10.1007/s13369-022-07117-5](https://doi.org/10.1007/s13369-022-07117-5).
- [35] M.N. Sultana and N.R. Dhar. Hybrid GRA-PCA and modified weighted TOPSIS coupled with Taguchi for multi-response process parameter optimization in turning AISI 1040 steel. *Archive Mechanical Engineering*, 68(1):23–49, 2021. doi: [10.24425/ame.2020.131707](https://doi.org/10.24425/ame.2020.131707).
- [36] K. Kumar and R.K. Verma. Measurement and evaluation of delamination factors and thrust force generation during drilling of multiwall carbon nanotube (MWCNT) modified polymer laminates. *Archive Mechanical Engineering*, 69(2):269–300, 2022. doi: [10.24425/ame.2022.140417](https://doi.org/10.24425/ame.2022.140417).
- [37] N.L. Bhirud and R.R. Gawande. Optimization of process parameters during end milling and prediction of work piece temperature rise. *Archive Mechanical Engineering*, 64(3):327–346, 2017. doi: [10.1515/meceng-2017-0020](https://doi.org/10.1515/meceng-2017-0020).
- [38] M.S. Węglowski. Experimental study and response surface methodology for investigation of FSP process. *Archive Mechanical Engineering*, 61(4):539–552, 2014. doi: [10.2478/meceng-2014-0031](https://doi.org/10.2478/meceng-2014-0031).
- [39] S. Prabhu and B.K. Vinayagam. Multiresponse optimization of EDM process with nanofluids using TOPSIS method and genetic algorithm. *Archive Mechanical Engineering*, 63(1):45–71, 2016. doi: [10.1515/meceng-2016-0003](https://doi.org/10.1515/meceng-2016-0003).
- [40] Y. Touggui, S. Belhadi, A. Uysal, M. Temmar, and M.A. Yallese. A comparative study on performance of cermet and coated carbide inserts in straight turning AISI 316L austenitic stainless steel. *International Journal of Advanced Manufacturing Technology*, 112:241–260, 2021. doi: [10.1007/s00170-020-06385-5](https://doi.org/10.1007/s00170-020-06385-5).
- [41] A. Laouissi, M.A. Yallese, A. Belbah, S. Belhadi, and A. Haddad. Investigation, modeling, and optimization of cutting parameters in turning of grey cast iron using coated and uncoated silicon nitride ceramic tools. Based on ANN, RSM, and GA optimization. *International Journal of Advanced Manufacturing Technology*, 101:523–548, 2019. doi: [10.1007/s00170-018-2931-8](https://doi.org/10.1007/s00170-018-2931-8).
- [42] A. Laouissi, M.M. Blaoui, H. Abderazek, M. Nouioua, and A. Bouchoucha. Heat treatment process study and ANN-GA based multi-response optimization of C45 steel mechanical properties. *Metals and Materials International*, 28:3087–3105, 2022. doi: [10.1007/s12540-022-01197-6](https://doi.org/10.1007/s12540-022-01197-6).
- [43] H. Ganesan and G. Mohankumar. Optimization of machining techniques in CNC turning centre using genetic algorithm. *Arabian Journal for Science and Engineering*, 38:1529–1538, 2013. doi: [10.1007/s13369-013-0539-8](https://doi.org/10.1007/s13369-013-0539-8).
- [44] G. Özden, M.Ö. Öteyaka, and F.M. Cabrera. Modeling of cutting parameters in turning of PEEK composite using artificial neural networks and adaptive-neural fuzzy inference systems. *Journal of Thermoplastic Composite Materials*, 36(2):493–509, 2023. doi: [10.1177/08927057211013070](https://doi.org/10.1177/08927057211013070).